ChemComm

COMMUNICATION

View Article Online
View Journal | View Issue

Cite this: *Chem. Commun.*, 2020, **56**, 14841

Received 27th August 2020,
Accepted 2nd November 2020

DOI: 10.1039/d0cc05786j

rsc.li/chemcomm

Probing the peripheral role of amines in photo- and electrocatalytic H_2 production by molecular cobalt complexes†

Dependu Dolui, [a] Ab Qayoom Mir [a] and Arnab Dutta *[ab]

The incorporation of amine functionality in the periphery of a synthetic cobaloxime core induces excellent photo-(TON 180) and electrocatalytic H_2 production (TOF 4330 s^{-1}) in aqueous solution. The primary amine group displays a superior influence on the catalysis compared to a secondary amine group with an analogous cobaloxime template.

The emergence of H_2 as an energy vector for the renewable energy economy has promoted the boom of synthetic H_2 evolution reaction (HER) catalysts.[1] Hydrogenase enzyme produces H_2 in aqueous solution with remarkable pace and efficiency. The presence of a protein scaffold surrounding the active site plays crucial roles in achieving this feat by regulating the substrate (H^+/e^-) and product (H_2) movement along with the structural dynamics of the metal core.[2] Hence, this protein structure, also known as the outer coordination sphere (OCS), is key in imitating the enzymatic HER efficiency.[3,4] Shaw and co-workers pioneered incorporating a synthetic OCS feature in the molecular catalyst design by precisely positioning amino acids and peptide motifs around the central metal framework to significantly improve the HER performance.[5,6] The strategic arrangement of the basic functionalities and delicate modification of the primary coordination sphere allowed the evolution of synthetic nickel-catalysts capable of even reversible H^+/H_2 interconversion, a hallmark of enzyme catalysis.[7,8] However, the intrinsic oxygen sensitivity of such catalysts has cast doubts on their long-term practical usability.

The inherent oxygen tolerance of cobaloxime[cobalt-(dimethylglyoxime)$_2$] complexes prompted their usage as an alternative solution. Cobaloximes exhibit moderate H_2 production when an N-heterocyclic axial donor (such as pyridine or imidazole) is appended to cobalt.[9–11] The photo- or electrocatalytic HER activity of cobaloxime derivatives displays a promising improvement in catalysis in the presence of protein, metallopeptide, cyclodextrin, and even metal–organic framework-based OCS features.[12–15] However, the bulkiness of the surrounding architectures has restricted the detailed analysis of their durable catalytic performance.[16] We have recently anchored natural amino acids and their derivatives *via* the axial N-heterocycle to generate minimal but essential OCS features around a cobaloxime core, which significantly improved both its photo- and electrocatalytic H_2 production in aqueous media.[17,18] A close look into the structure–function relationship of these complexes revealed the plausible formation of water and the accompanying anion-mediated proton relay around the complexes to trigger a rapid proton movement under catalytic conditions.

Amine groups are considered vital factors in crafting an interactive proton relay in biology. The mercurial influence of the pendant amine on the [FeFe]-hydrogenase activity has motivated the evolution of synthetic Fe- and Ni-based analogs.[19,20] In those complexes, variable protic nitrogenous functionalities such as N-heterocyclic motifs and secondary and tertiary amines were utilized to enhance the catalytic H_2 production.[21–23] However, the exclusive use of such functionalities for a cobalt-based H_2 production catalyst template is rare. Our previous study highlighted the potential involvement of peripheral amines around a cobaloxime template, although their effect was masked in the presence of other fringe basic functionalities (carboxylate and phenol). Hence, cobaloximes containing only peripheral amines are required to unravel their impact as an OCS feature.

In the present study, we have developed a series of three complexes bearing the same cobaloxime template and varying only in the identity of the OCS feature (Scheme 1). Among them, the control complex contains an aliphatic ethyl group (**C1**), while the others include either a primary (**C2**) or a secondary amine group (**C3**) in the periphery.

All these complexes were synthesized by the conventional stoichiometric addition of pyridine derivatives to the methanolic solution of [cobalt-(dimethylglyoxime)$_2$] (ESI†).[17] The optical spectra

[a] *Chemistry Discipline, Indian Institute of Technology Gandhinagar, Palaj 382355, India. E-mail: arnabdutta@chem.iitb.ac.in*
[b] *Chemistry Department, Indian Institute of Technology Bombay, Powai 400076, India*

† Electronic supplementary information (ESI) available: Synthetic procedures, experimental procedures, and additional figures. CCDC 2040107. For ESI and crystallographic data in CIF or other electronic format see DOI: 10.1039/d0cc05786j

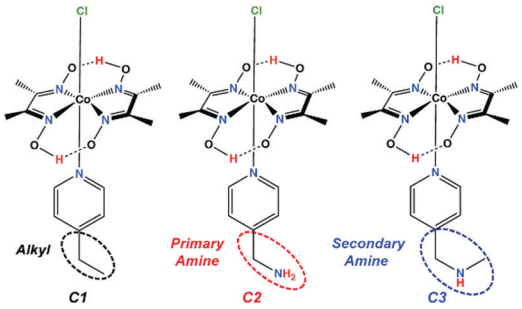

Scheme 1 Schematic structures of the complexes **C1–C3**. The dotted ellipses highlight the outer coordination sphere (OCS) functionalities around the cobaloxime core.

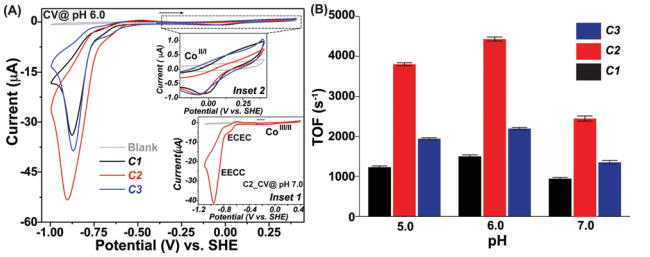

Fig. 1 (A) Comparative cyclic voltammogram (CV) data for **C1** (black trace), **C2** (red trace), and **C3** (blue trace), and blank solution (grey trace) recorded at pH 6.0, while the inset 1 and 2 exhibit the CV response for **C2** (red trace) in pH 7.0 and the Co(III/II) stoichiometric signal for **C1–C3** at pH 6.0 (scan rate 1 V s^{-1}). (B) Variation of the electrocatalytic H_2 production TOF values for **C1** (black bar), **C2** (red bar), and **C3** (blue bar) recorded in aqueous solution ranging from pH 5.0 to 7.0. The horizontal arrows display the initial scan direction. The standard deviation values were calculated from at least three independent experimental data.

of these complexes exhibited the salient features of ligand-to-metal charge transfer (LMCT) (~350 nm) and d–d transition bands (~500–600 nm), which suggests the formation of an axial pyridine motif bound cobaloxime (Co–N_5) core (Fig. S1A and Table S1, ESI†),[24] which was supported further by the appearance of a characteristic absorption band at ~500 cm^{-1} in the ATR-FTIR spectra (Fig. S1B and Table S1, ESI†).[25] The corresponding ^1H and ^{13}C NMR spectral data of **C1–C3** depicted that the axially bound pyridine derivatives remain intact even after generating the complexes (ESI†). The ^1H NMR data also displayed a highly down-field shifted signal (~18.5 ppm), indicating the formation of a hydrogen-bonded oxime network in the primary coordination sphere of the complexes (ESI†).[17] The single-crystal structure of **C2**, grown in organic media, indicates the interaction between the primary amine with a cobaloxime core leading to the formation of a heterodimer. However, the protonation of that primary amine will ensure the generation of only an $N_{pyridine}$-linked cobaloxime core in aqueous solution (pH $\leq$ 7) (Fig. S2 and Table S2, ESI†).

The electrochemical properties of the complexes were first inspected in polar aprotic acetonitrile media, where **C1–C3** displayed two distinct signatures corresponding to quasi-reversible Co(III/II) and reversible Co(II/I) redox processes, respectively (Fig. S3 and Table S1, ESI†).[9,25] The Co(III/II) reduction peak for **C1** shifted by ~100 mV towards a more negative potential (−1.11 V *vs.* $FeCp_2^{+/0}$) compared to amine-containing **C2** and **C3** (~−1.0 V *vs.* $FeCp_2^{+/0}$) in acetonitrile. The weakened $N_{pyridine} \rightarrow Co$ σ-donation for **C2** and **C3**, due to the presence of electron-withdrawing amine groups, is presumably the reason behind this variation.[16,24]

The inclusion of the amine moiety improved the solubility of both **C2** and **C3**, compared to moderately water-soluble **C1**. Hence, it was possible to probe the redox properties for all the complexes in an aqueous solution. The CV data for all the complexes (**C1–C3**) exhibited three distinct features during the reductive scan in pH 7.0 solution (Fig. 1A (inset 1) and Fig. S4, ESI†). The first reduction peak was noticed at −0.1 V (*vs.* SHE) during the scan, starting from a relatively positive direction. This signal belongs to a quasi-reversible stoichiometric Co(III/II) redox step analogous to the previously reported water-soluble pyridine-bound cobaloximes.[17,24] An irreversible reductive response was observed next at −0.7 V (*vs.* SHE). This signal is catalytic in nature (for the HER activity), and it originated due to an ECEC catalytic mechanism that revolved around the Co(II)-centre (Fig. S5, ESI†).[11,17,26] A relatively sharper catalytic H_2 production signal was observed upon further reducing the potential starting from −0.85 V (*vs.* SHE). This dominant catalytic response originated from the Co(I)-centred EECC mechanism (Fig. S5, ESI†).[17,26]

The ratio of the catalytic current (i_{cat}) and the stoichiometric signal (from the Co(III/II) peak) (i_p) was utilized (eqn (S1), ESI†) for evaluating the catalytic rate (k_{obs} or the turn over frequency/TOF) of H_2 production by these complexes. On the other hand, the parameter overpotential signifies the energy efficiency of these electrocatalysts that is measured as a difference between the thermodynamic H^+/H_2 couple (E_{H^+/H_2}) and the potential of the half maxima of the catalytic current ($E_{cat/2}$) (eqn (S2), ESI†). The complexes exhibited weak H_2 production *via* the ECEC mechanism at a relatively positive potential, while a rapid HER catalysis, proceeding through the EECC mechanism, was observed at a comparatively negative potential. Among the three complexes, the primary amine-containing **C2** displayed the best EECC-mechanistic HER rate (2448 s^{-1}) followed by secondary amine appended **C3** (1350 s^{-1}) in pH 7.0 aqueous solution (Fig. 1B and Table 1). The amine-deprived control complex **C1** was the slowest H_2 producer (TOF 930 s^{-1}) under similar conditions, which is similar to the unsubstituted pyridine-coordinated cobaloxime.[17] Although there was not much difference in the overpotential requirement for these complexes during the ECEC mechanism-based HER, they behaved differently during the fast EECC type catalysis. In the latter condition, **C2** exhibited better energy efficiency than **C1** and **C3** (Table 1).

As the pH of the solution is lowered to 6.0, the ECEC-type HER signal became negligible for **C1–C3** (Fig. 1A). On the contrary, the EECC-based H_2 production signal improved under this condition. All the complexes displayed their fastest catalytic rate at pH 6.0 in the order of **C2** > **C3** > **C1**, analogous to the previous study at pH 7.0. Here, **C2** reached the maximum TOF of 4331 s^{-1}, which is one of the highest HER rates for cobaloxime derivatives containing only one basic functionality (primary amine for **C2**) in the OCS. The primary amine-containing **C2**

again demonstrated a lower overpotential requirement (448 mV) among all the complexes (Table 1).

Further reduction in the pH of the solution (pH 5.0) truncated the dominant EECC catalytic signal for all the complexes, while the catalytic response originating from the ECEC mechanism remained inconsequential (Fig. 1B and Fig. S6, ESI†). **C2** continued to showcase its superior energy efficiency for H_2 production over **C1** and **C3**, even at pH 5.0 (Table 1). The complementary spectroelectrochemical experiments exhibited the continuous presence of the $N_{pyridine} \rightarrow Co$ LMCT band during the reducing scan which suggested the stability of the $Co–N_{pyridine}$ axial bond even under catalytic conditions (Fig. S7, ESI†).

The catalytic response for the complexes decreased significantly below pH 5.0, largely due to the protonation-induced depletion of the oxime hydrogen-bonded network present in the primary coordination sphere.[17] Hence, no HER electrocatalysis was performed for **C1–C3** at pH $<$ 5.0. Chronocoulometric experiments were performed for all the complexes at pH 6.0 (at their peak catalytic performance). They exhibited robust homogeneous catalytic activity with significant H_2 production during this bulk electrolysis, which was detected by complementary gas chromatography (GC) experiments (Fig. S8, ESI†). The catalyst solution's optical spectra exhibited a minimal change which indicated the stability of **C1–C3** during the chronocoulometric experiments (Fig. S9, ESI†). The plastic chip working electrode used during the experiment was further probed *via* field emission scanning electron microscopy in conjunction with energy-dispersive X-ray spectroscopy (FE-SEM/EDS).[27] The results from this data displayed no cobalt deposition on the electrode material which indicated the robustness of the complexes under electrocatalytic HER conditions (Fig. S10, ESI†).

The electrochemical data established **C2** as the best electrocatalyst for aqueous H_2 production in this current series of complexes, followed by **C3**. The direct participation of the peripheral amine functionalities in H^+ exchange during the catalysis is believed to be one of the chief reasons behind the improved reactivity of **C2** and **C3** over **C1**. Two-dimensional NMR technique exchange spectroscopy (EXSY) was performed to probe this hypothesis further. The **C1** complex only displayed proton exchange between the hydrogen-bonded oxime groups with the bulk water with no participation from the alkyl-based OCS, analogous to the cobaloxime containing unsubstituted pyridine ligand (Fig. S11, ESI†).[17] The presence of the primary amine group in **C2** ensures a three-way proton exchange between the oximes, $–NH_2$, and bulk water, which was evident from the appearance of multiple cross-peaks in the EXSY spectrum (Fig. 2). Analogously, the EXSY data of **C3** depicted interactive proton hopping involving secondary amine, oxime, and external water molecules (Fig. S12, ESI†). This series of two-dimensional NMR experiments revealed the dynamic nature of the amine functionalities dangling from the axial pyridine motif, which play a vital role in amplifying the proton traffic between the bulk solution and the cobaloxime core. The EXSY experiment with the solution containing **C2** and a stoichiometric amount of **L2** ligand did not exhibit any new cross-peaks which indicated the intramolecular interaction between the protic functionalities present in the cobaloxime framework. This hypothesis was corroborated further by the lack of improvement in the catalytic HER behavior when the external **L2** ligand was added to the unsubstituted pyridine-linked cobaloxime (Fig. S13, ESI†). The addition of D_2O instead of H_2O significantly affects the electrochemical behavior of **C2** in organic media, which highlights the vital role of water molecules in inducing intramolecular proton exchange (Fig. S14, ESI†).

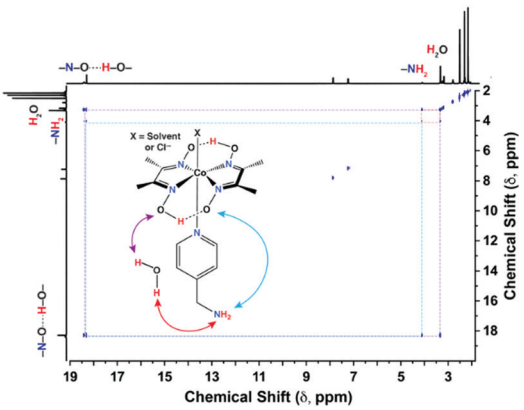

Fig. 2 Two-dimensional EXSY spectra recorded for **C2** in d_6-DMSO, containing a minute amount of water, with 350 ms mixing time at 298 K. The dotted lines connecting the cross peaks demonstrate the exchange between primary amine–oxime (sky blue trace), primary amine–water (red trace), and oxime–water (violet trace).

Thus, the inclusion of amine groups in the OCS of cobaloximes resulted in improved electrocatalytic H_2 evolution in aqueous solution. The complexes **C1–C3** were probed further under

Table 1 Comparative electro- and photocatalytic HER data for **C1–C3**

	Electrocatalytic HER						
	pH 5.0		pH 6.0		pH 7.0		Photo-catalytic HER (TON *vs.* PS)[c]
Complex	TOF[a] (s^{-1})	OP[b] (mV)	TOF (s^{-1})	OP (mV)	TOF (s^{-1})	OP (mV)	
C1	1228 ± 33	465 ± 5	1500 ± 37	459 ± 2	930 ± 41	476 ± 2	128
C2	3800 ± 35	457 ± 5	4331 ± 52	448 ± 2	2448 ± 65	455 ± 2	180
C3	1940 ± 28	488 ± 5	2195 ± 31	464 ± 2	1350 ± 45	496 ± 2	146

[a] TOF: Turnover frequency. [b] OP: Overpotential. [c] PS: Photosensitizer.The standard deviation values were calculated from at least three independent experimental data.

photocatalytic conditions to gauge the effect of these peripheral amine functionalities beyond the electrochemical conditions. Cobaloximes, axially coordinated to pyridine derivatives, are known for photo-driven H_2 production in conjunction with a photosensitizer (PS) Eosin-Y (Fig. S15, ESI† inset) and a sacrificial electron-donor triethanolamine (TEOA) in the presence of at least 30% of organic solvents.[28] However, its photocatalytic HER activity was slow (TON ~220 over 30 hours of irradiation), while significant photo-degradation of the complex was noticed. The inclusion of protic carboxylic acid groups around the pyridine improved the light-driven H_2 production; however, the long-term stability of cobaloxime derivatives remained an issue.[29] Here, the photocatalytic H_2 production by complexes **C1–C3** was investigated in pure aqueous solution (pH 7.0) in the presence of a typical setup consisting of a Eosin-Y and TEOA mixture.

All the complexes exhibited significant H_2 production in neutral aqueous solution under visible light irradiation (λ_{ex} 335–610 nm) (Fig. S15A, ESI†). During this experiment, the evolution of H_2 was monitored periodically by GC (Fig. S15B, ESI†), which exhibited no lag period or photo-degradation of the sample during 6 hours of irradiation. Analogous to the electrochemical HER results, the same trend of **C3** > **C2** > **C1** remained valid even for the photocatalytic H_2 production performance. **C2** exhibited the maximum TON of 180 over 6 hours of photo-irradiation, while **C1** and **C3** exhibited 128 and 146 turnovers, respectively (Fig. S15A, ESI† and Table 1). Thus, the presence of a primary amine proves to be critical in establishing one of the best photocatalytic HER performances by $N_{pyridyl}$-linked cobaloximes under pure aqueous conditions.[18] The complementary dynamic light scattering (DLS) experiments on either side of photocatalysis confirmed the homogenous nature of the catalyst during the study (Fig. S16, ESI†).

In summary, the current study of three cobaloxime derivatives depicts the importance of the strategic incorporation of amine functionalities as an OCS feature, which boosted the catalytic H_2 production by an otherwise identical synthetic catalyst. The primary amine-decorated **C2** illustrated one of the fastest electrocatalytic H_2 production rates for the cobaloxime-pyridine template containing a solitary basic group in the periphery. The primary amine group (**C2**) proves to be superior in enhancing both the photo- and electrocatalytic HER performance compared to the secondary amine (**C3**), presumably due to the improved proton exchange. Hence, this set of complexes has allowed us to obtain a snapshot of the intricate role of peripheral amines in remotely influencing the catalytic active site to develop the next-generation artificial catalyst design strategies.

Conflicts of interest

There are no conflicts to declare.

Notes and references

1 V. Artero, *Nat. Energy*, 2017, **2**, 1–6.
2 B. Ginovska-Pangovska, M.-H. Ho, J. C. Linehan, Y. Cheng, M. Dupuis, S. Raugei and W. J. Shaw, *Biochim. Biophys. Acta, Bioenerg.*, 2014, **1837**, 131–138.
3 B. Ginovska-Pangovska, A. Dutta, M. L. Reback, J. C. Linehan and W. J. Shaw, *Acc. Chem. Res.*, 2014, **47**, 2621–2630.
4 J. A. Laureanti, M. O'Hagan and W. J. Shaw, *Sustainable Energy Fuels*, 2019, **3**, 3260–3278.
5 A. Jain, S. Lense, J. C. Linehan, S. Raugei, H. Cho, D. L. DuBois and W. J. Shaw, *Inorg. Chem.*, 2011, **50**, 4073–4085.
6 M. L. Reback, G. W. Buchko, B. L. Kier, B. Ginovska-Pangovska, Y. Xiong, S. Lense, J. Hou, J. A. S. Roberts, C. M. Sorensen, S. Raugei, T. C. Squier and W. J. Shaw, *Chem. – Eur. J.*, 2014, **20**, 1510–1514.
7 A. Dutta, D. L. DuBois, J. A. S. Roberts and W. J. Shaw, *Proc. Natl. Acad. Sci. U. S. A.*, 2014, **111**, 16286–16291.
8 N. Priyadarshani, A. Dutta, B. Ginovska, G. W. Buchko, M. O'Hagan, S. Raugei and W. J. Shaw, *ACS Catal.*, 2016, **6**, 6037–6049.
9 M. Razavet, V. Artero and M. Fontecave, *Inorg. Chem.*, 2005, **44**, 4786–4795.
10 F. Lakadamyali, M. Kato, N. M. Muresan and E. Reisner, *Angew. Chem., Int. Ed.*, 2012, **51**, 9381–9384.
11 D. Dolui, S. Ghorai and A. Dutta, *Coord. Chem. Rev.*, 2020, **416**, 213335.
12 M. Bacchi, G. Berggren, J. Niklas, E. Veinberg, M. W. Mara, M. L. Shelby, O. G. Poluektov, L. X. Chen, D. M. Tiede, C. Cavazza, M. J. Field, M. Fontecave and V. Artero, *Inorg. Chem.*, 2014, **53**, 8071–8082.
13 S. R. Soltau, P. D. Dahlberg, J. Niklas, O. G. Poluektov, K. L. Mulfort and L. M. Utschig, *Chem. Sci.*, 2016, **7**, 7068–7078.
14 M. Kato, K. Kon, J. Hirayama and I. Yagi, *New J. Chem.*, 2019, **43**, 10087–10092.
15 S. Roy, Z. Huang, A. Bhunia, A. Castner, A. K. Gupta, X. Zou and S. Ott, *J. Am. Chem. Soc.*, 2019, **141**, 15942–15950.
16 D. Dolui, S. Khandelwal, P. Majumder and A. Dutta, *Chem. Commun.*, 2020, **56**, 8166–8181.
17 D. Dolui, S. Khandelwal, A. Shaik, D. Gaat, V. Thiruvenkatam and A. Dutta, *ACS Catal.*, 2019, **9**, 10115–10125.
18 D. Dolui, S. Das, J. Bharti, S. Kumar, P. Kumar and A. Dutta, *Cell Rep. Phys. Sci.*, 2020, **1**, 100007.
19 G. Berggren, A. Adamska, C. Lambertz, T. R. Simmons, J. Esselborn, M. Atta, S. Gambarelli, J.-M. Mouesca, E. Reijerse, W. Lubitz, T. Happe, V. Artero and M. Fontecave, *Nature*, 2013, **499**, 66–69.
20 D. L. DuBois, *Inorg. Chem.*, 2014, **53**, 3935–3960.
21 M. E. Ahmed, S. Dey, M. Y. Darensbourg and A. Dey, *J. Am. Chem. Soc.*, 2018, **140**, 12457–12468.
22 R. Zaffaroni, W. I. Dzik, R. J. Detz, J. I. van der Vlugt and J. N. H. Reek, *Eur. J. Inorg. Chem.*, 2019, 2498–2509.
23 S. Lense, A. Dutta, J. A. S. Roberts and W. J. Shaw, *Chem. Commun.*, 2014, **50**, 792–795.
24 D. W. Wakerley and E. Reisner, *Phys. Chem. Chem. Phys.*, 2014, **16**, 5739–5746.
25 A. Panagiotopoulos, K. Ladomenou, D. Sun, V. Artero and A. G. Coutsolelos, *Dalton Trans.*, 2016, **45**, 6732–6738.
26 E. S. Rountree, D. J. Martin, B. D. McCarthy and J. L. Dempsey, *ACS Catal.*, 2016, **6**, 3326–3335.
27 M. Perween, D. B. Parmar, G. R. Bhadu and D. N. Srivastava, *Analyst*, 2014, **139**, 5919–5926.
28 T. Lazarides, T. McCormick, P. Du, G. Luo, B. Lindley and R. Eisenberg, *J. Am. Chem. Soc.*, 2009, **131**, 9192–9194.
29 J. Wang, C. Li, Q. Zhou, W. Wang, Y. Hou, B. Zhang and X. Wang, *Dalton Trans.*, 2015, **44**, 17704–17711.

